Chapter 5

A Planar Low-Profile Gain-Enhanced CPW-Fed Slotted Patch Antenna Using AMC Surface

5.1. Introduction

This chapter discusses a metasurface (MS) antenna employing the properties of the artificial magnetic conductor (AMC). An AMC is a type of MS that introduces an in-phase reflection within the desired frequency band-gap [101]-[103]. Sievenpiper proposed the AMC in 1999 as an artificial microstructure material with a special surface structure [16]-[17]. It is created by etching a copper-clad plate and has a high-impedance surface structure as well as very small tangential magnetic fields. When this material is applied to an antenna, the high impedance at the surface of the AMC allows for simultaneous control of surface wave suppression and zero phase reflection [16]-[17]. In practice, AMCs lead electromagnetic waves into the upper-half space by crossing the 0° reflection phase at only one frequency (for one resonant mode) [101]-[103]. The operational bandwidth of an AMC is generally defined as –90° to 90° on either side of the central frequency where the phase values of the surface would not cause destructive interference between direct and reflected waves [101]-[103]. The AMC structures have been extensively studied as a reflector instead of the ground plane, which has shown exceptional benefits in terms of suppressing back radiation, enhancing gain, broadening bandwidth, and also allowing for the miniaturization of the antenna profile [102]-[105]. Recently, various technologies, such as the use of parasitic elements and inserting slots in the radiating structure, have been implemented to improve the performance of the impedance bandwidth of the antenna [105]–[108]. Several feeding methodologies, such as microstrip line fed, inset-fed, edge fed, coaxial probe fed, coplanar waveguide-fed (CPW-fed), and so on, have been used in antenna structures to improve antenna features [96–108]. In wireless applications, the CPW-fed slot antenna is more practical and conspicuous for multiband or wideband features; although, the antenna offers low gain [114], [188].

In this chapter, the configuration consists of a CPW-fed slotted patch antenna and a 7×7 order AMC surface separated by a layer of teflon. Teflon has good electrical properties and provides mechanical robustness to the antenna, as well as resistant to temperature variation [181]. Here, the radiating patch is placed on top of the first dielectric, while the MS layer has been positioned on top of the second dielectric. The MSA operates at 2.34 GHz and 8.94 GHz while offering the maximum return loss of 42 dB at 8.94 GHz. This antenna provides fractional bandwidths of 6.8% and 53.8% at the two operational frequencies. The prototype exhibits directional radiation features along with the E- and H-planes in which the maximum achievable gain of 9.1 dBi and radiation efficiency of 91.2% at 11.51 GHz. The proposed prototype has been fabricated, and the experimentally measured parameters agree well with the simulated values.

5.2. Design of the Metasurface Antenna

The proposed antenna consists of a slotted patch fed by CPW and a 7×7 order MS in which the patch and AMC reflector are constructed on two distinct FR4 dielectric substrates (relative permittivity of 4.4 and loss tangent of 0.025) of 1.6 mm thickness, separated by a 5 mm thick teflon layer (loss tangent = 0.001 and relative permittivity = 2.1). The AMC unit cell comprises a centre patch surrounded by a square ring-shaped patch. Fig. 5.1 depicts a three-dimensional schematic representation of the suggested AMC-based MS structure. Further, the radiating patch and 7×7 order AMC surface of the proposed MSA are depicted in Figs. 5.2(a) and 5.2(b), respectively. Fig. 5.3 illustrates the comprehensive analysis of the AMC unit cell, whereas Figs. 5.4(a) and 5.4(b) demonstrate the reflection characteristics of the radiating patch and the MSA, respectively. The proposed prototype has been analyzed and optimized using Ansys HFSS [166].

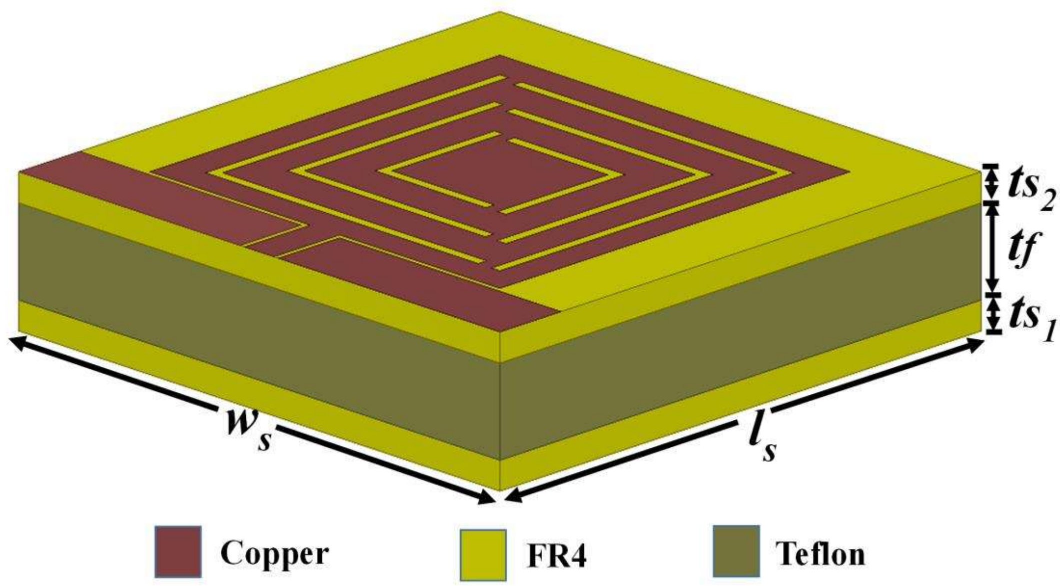

Fig. 5.1. The 3D view of the proposed AMC based metasurface structure [Designed parameters: $w_s = l_s$ =33 mm, $t_{s1} = t_{s2}$ =1.6 mm, t_f = 5 mm].

The three-dimensional design of the AMC unit cell is depicted in Fig. 5.3(a), which includes a centered patch surrounded by a square-shaped ring. The AMC surface is a copper-based conducting surface that is placed above the second FR4 substrate. The equivalent LC parallel resonance of the MS unit cell has been achieved by adjusting the space between the centre patch and the square ring-shaped patch surrounding it. The unit cell has been studied under periodic boundary conditions incorporating Ansys HFSS [166].

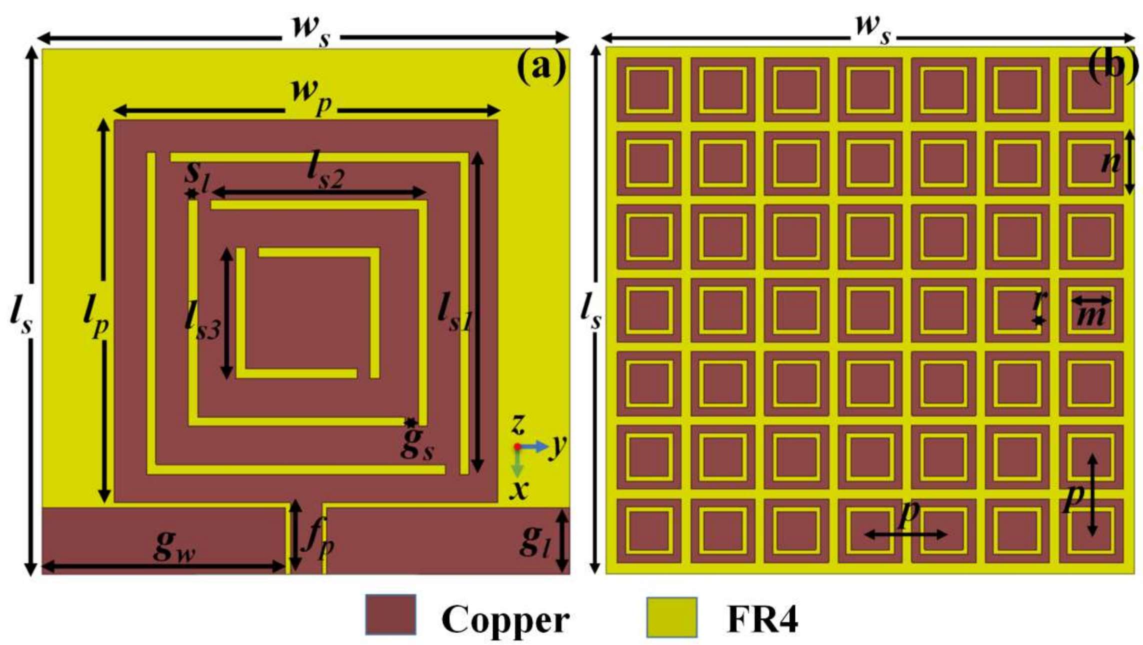

Fig. 5.2. Proposed AMC based MS antenna with (a) Radiating patch and (b) 7×7 order AMC surface [Designed parameters: $w_s = l_s$ =33 mm, $w_p = l_p$ =24 mm, g_l = 4.2 mm, g_w = 15.2 mm, f_p = 4.5 mm, l_{s1} = 14.2 mm, l_{s2} = 13.6 mm, l_{s3} = 8.2 mm, s_l = 0.6 mm, g_s = 0.8 mm, p = 4.6 mm, m = 2.4 mm, n = 4 mm, r =0.3 mm].

The unit cell's reflection phase characteristics are shown in Fig. 5.3(b), where the unit cell is designed with zero-crossing phases to improve the radiation characteristics and achieve a high gain. Additionally, in Figs. 5.3(c) and 5.3(d), the effective permittivity and permeability of the MS layer have been thoroughly investigated by examining the reflection and transmission properties of the unit cell [47]-[49]. The AMC-based MS layer acts as a left-handed material over the frequency range 1-3.8 GHz and 8.8-11 GHz. In the next step, the homogeneity of the metasurface has been taken into account while designing the AMC unit cells. The equivalent input impedance of an MS unit element can be expressed as the parallel combination of the impedances of the periodic pattern and the grounded dielectric layer impedance. There is an improvement in bandwidth due to the combined effect of slot impedance in the patch and the MS.

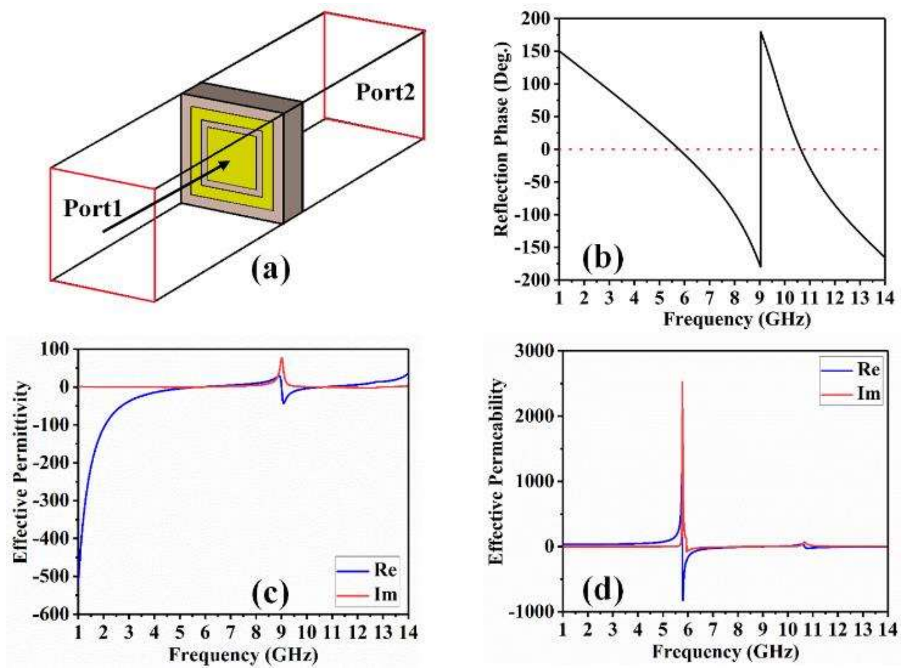

Fig. 5.3. (a) The 3D view (b) Reflection Phase characteristics (c) Effective permittivity and (d) Effective permeability of the unit cell.

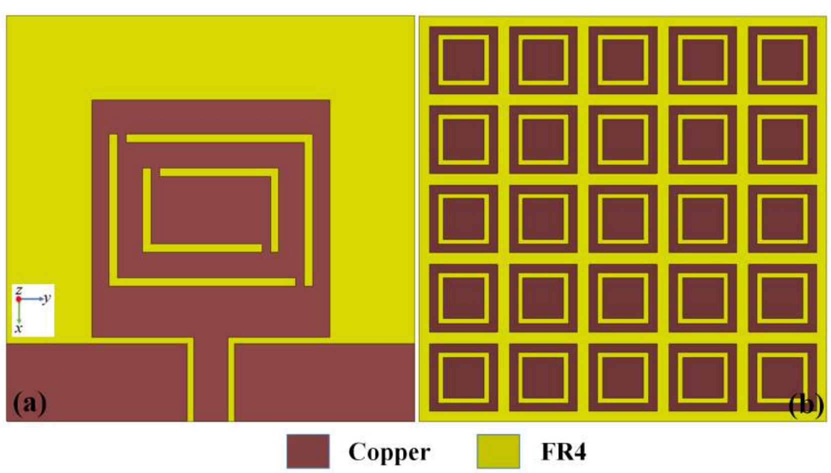

Fig. 5.4. AMC-based MS antenna with (a) Radiating patch and (b) 5×5 order AMC surface.

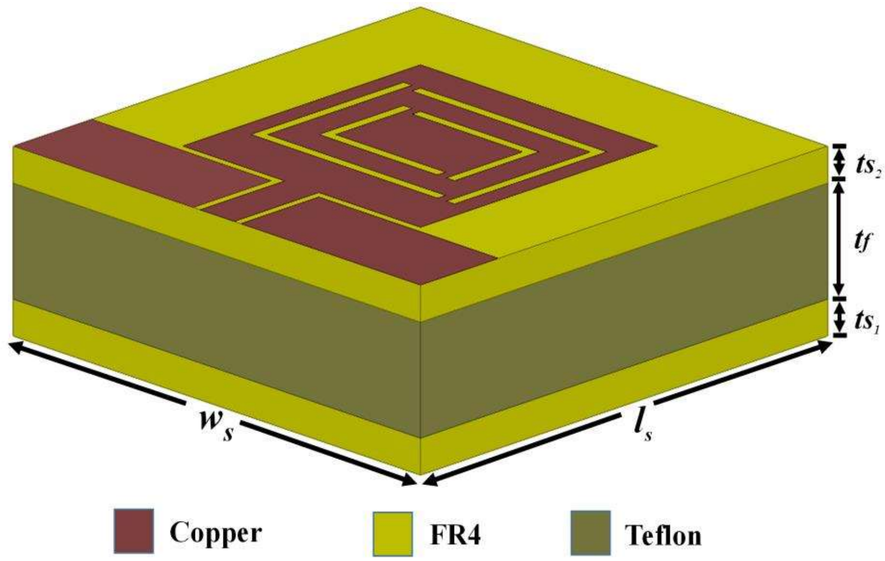

Fig. 5.5. The 3D view of the AMC-based structure with 5×5 order MS.

Initially, a simple microstrip patch antenna has been used to initiate the design process; however, later on, the patch antenna has been modified by introducing CPW-feed into the patch for performance improvement as depicted in Fig. 5.4. Here, two pairs of parasitic L-shaped slot elements have been included in the patch to improve the frequency of operations and bandwidth. The CPW-fed patch antenna produces enhanced bandwidths from 3.92 GHz-4.61 GHz and 9.11 GHz-9.44 GHz with a maximum return loss of 29 dB at 4.36 GHz. Next, a 5×5 order MS has been incorporated with a CPW-fed slotted patch in which the MS has been placed below the radiating patch with a different FR4 dielectric. A layer of 5 mm thick teflon dielectric has been placed in between two FR4 dielectrics, forming a superstrate structure. The three-dimensional view of the 5×5 order MS with the radiating patch has been shown in Fig. 5.5.

The loading of the AMC layer results in a triple-band response of the antenna operating over the bands 3.82-4.30 GHz, 8.55-9.02 GHz, and 11.71-12.56 GHz with the respective fractional bandwidths of 11.6%, 5.3%, and 7% at 4.13 GHz, 8.80 GHz and 12.01 GHz as evident from

Fig. 5.6. The maximum return loss of 36 dB has been achieved at 12.01 GHz. However, the observed bands in the antenna with two pairs of parasitic L-shaped slot elements with a 5×5 order AMC surface are narrow. As a result, an additional pair of parasitic L-shaped slot elements have been added to the radiating patch for the purpose of increasing bandwidth.

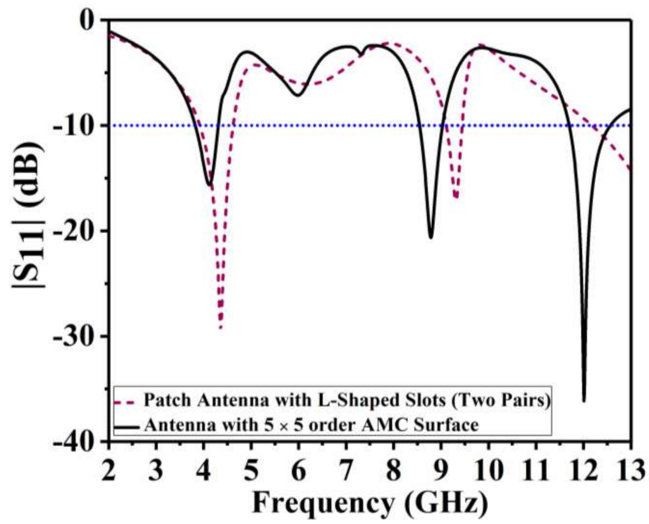

Fig. 5.6. The plot of $|S_{11}|$ (dB) with respect to the frequency of the antenna configuration shown in Fig. 5.4.

A further study in Case-I of Fig. 5.7 has been performed to examine the effects of three pairs of parasitic L-shaped slot elements without CPW-fed in the radiating patch. The patch incorporates parasitic L-shaped slot elements to increase the frequency of operations and bandwidth, and the reflection characteristics have been analyzed further in Fig. 5.8. The slotted patch resonates at multiple frequencies viz., 2.16 GHz, 6.73 GHz, 9.03 GHz, and 11.68 GHz with a maximum return loss of 36 dB at 6.73 GHz. The addition of CPW feeding with three pairs of L-shaped slots in Case-II has resulted in an improvement in the limitation of multiple resonances in Case-I of Fig. 5.8. This has been accomplished by increasing the number of L-shaped slots in Case-II of Fig. 5.8. The slotted patch has been integrated with

CPW feed in this design to improve antenna performance in terms of bandwidth and return loss. The parametric variation of the L-shaped slot width (s_l) designed in the patch is shown in Fig. 5.9. It has been observed that the antenna impedance is quite high at $s_l = 2$ mm.

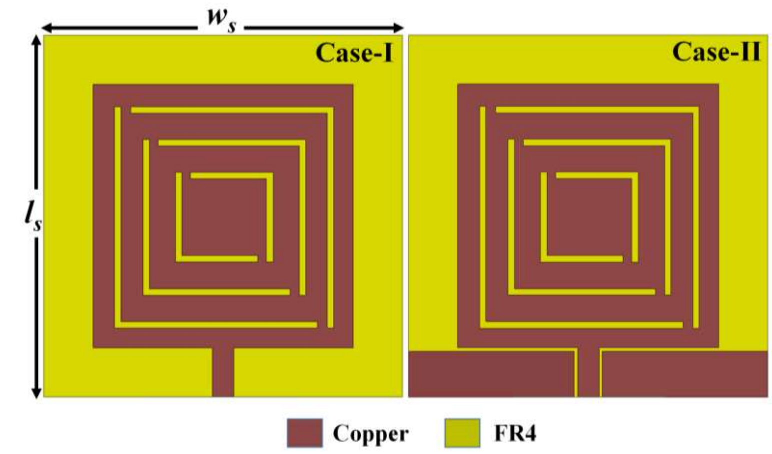

Fig. 5.7. Design steps of the conventional patch with different modifications.

The CPW-fed slotted patch antenna exhibits improved bandwidths from 2.31 GHz to 2.41 GHz, and 7.54 GHz to 10.37 GHz, with a maximum return loss of 31 dB at 7.73 GHz. Because of its improved properties, the antenna presented in Case-II of Fig. 5.8 has been classified as the conventional antenna.

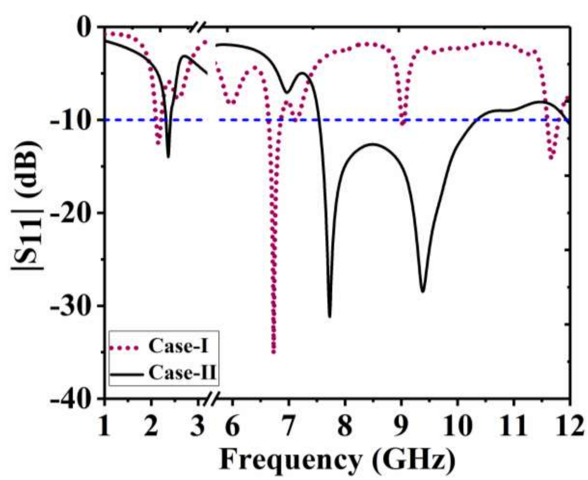

Fig. 5.8. The plot of reflection characteristics comparison with respect to the frequency of the different antenna configurations shown in Fig. 5.7.

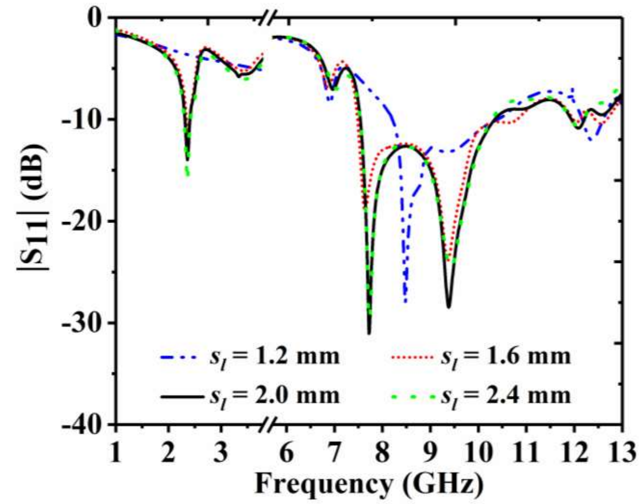

Fig. 5.9. The plot of $|S_{11}|$ (dB) versus frequency at s_l variations of the MS antenna.

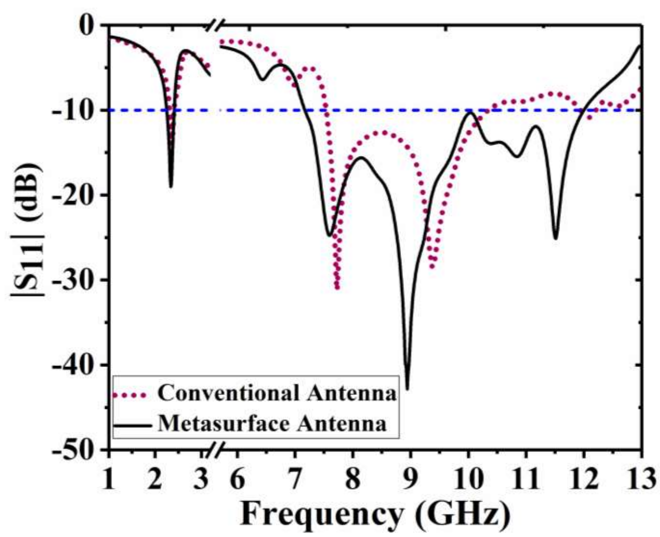

Fig. 5.10. The comparison of the reflection characteristics of the conventional antenna and the metasurface antenna with respect to frequency.

Thereafter, a 7×7 order MS has been combined with the CPW-fed slotted patch in which the MS has been placed below the radiating patch using a separate FR4 dielectric. A 5 mm thick dielectric layer of teflon has been sandwiched between the two FR4 dielectric layers in this design, forming a superstrate configuration. Positioning the AMC layer below the radiating patch in a superstrate design considerably improves antenna performance, as illustrated in Fig. 5.10. Here, the AMC-based MS antenna has been compared to the conventional antenna.

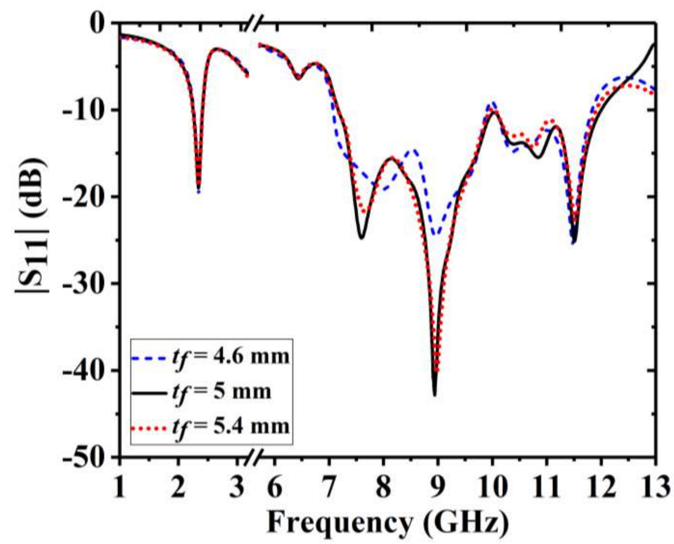

Fig. 5.11. The plot of $|S_{11}|$ (dB) versus frequency at t_f -variations of the MS antenna.

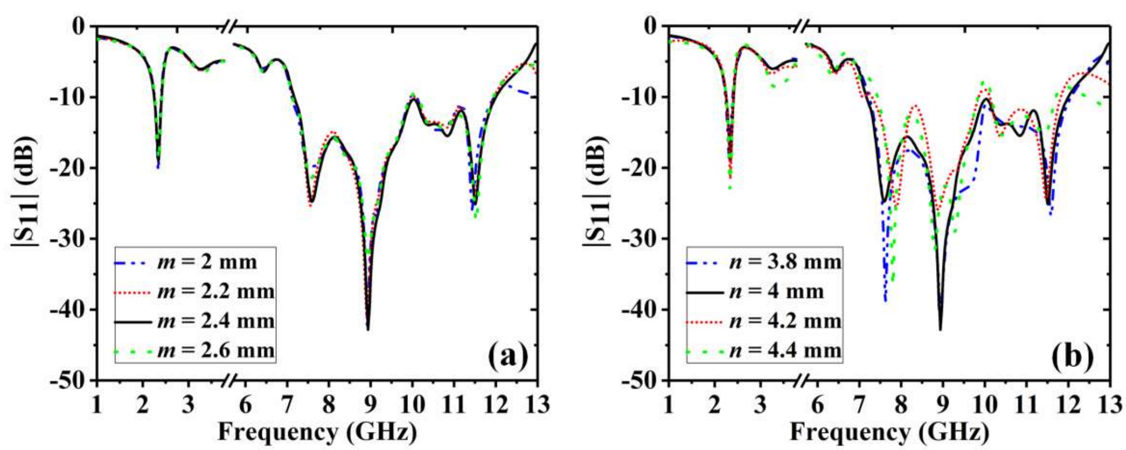

Fig. 5.12. Plot of $|S_{11}|$ (dB) with respect to frequency (GHz) (a) at different *m*-variations and (b) at different *n-variations*.

The analysis of the reflection characteristics of the MS antenna has been studied in Fig. 5.11 by varying the teflon height (t_f) across two substrate. At t_f = 5 mm, the MS antenna performs well in terms of impedance bandwidth and return loss. Moreover, the parametric study of the centre patch dimension (m) surrounded by a square ring-shaped patch dimension (n) and the gap between two consecutive unit cells along the horizontal and vertical directions (p) are shown in Fig. 5.12 and Fig. 5.13 respectively. It has been observed that at m = 2.4 mm, n = 4 mm, and p = 4.6 mm, the antenna exhibits good impedance matching with improved bandwidth.

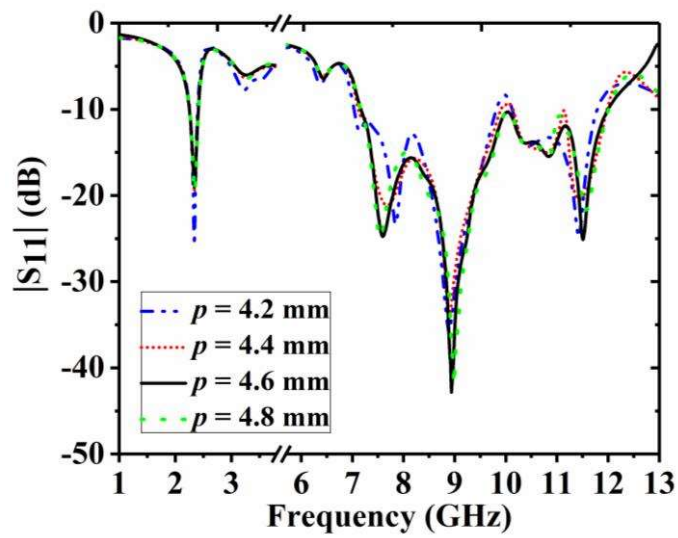

Fig. 5.13. The plot of $|S_{11}|$ (dB) versus frequency at p-variations of the MS antenna.

The basic difference between the antenna designed in Fig. 5.1 and Fig. 5.5 is that in Fig. 5.5, two pairs of parasitic L-shaped slot elements have been included in the patch to improve the frequency of operations and bandwidth. A 5×5 order MS has been incorporated with a CPW-fed slotted patch in which the MS has been placed below the radiating patch with a different FR4 dielectric. Here, the observed bands in the antenna with two pairs of parasitic L-shaped slot elements with a 5×5 order AMC surface are narrow and the separation between the co-polarized and cross-polarized radiation characteristics is not improved. As a result, an additional pair of parasitic L-shaped slot elements in the radiating patch and a 7×7 order AMC surface have been incorporated in Fig. 5.5 for further improvement in the impedance bandwidth and radiation characteristics. The increase of the L-shaped slot improves the antenna performance in terms of bandwidth and return loss. The CPW-fed slotted patch antenna exhibits improved bandwidths from 2.25-2.41 GHz, and 7.27-11.98 GHz, in which the antenna offers the respective fractional bandwidths of 6.8% and 53.8% at 2.34 GHz and 8.94 GHz. Moreover, a maximum return loss of 42 dB has been attained at 8.94 GHz. The proposed antenna achieves maximum realized gains of 9.2 dBi at 11.98 GHz.

5.3. Results and analysis

The designed antenna has been manufactured using the LPKF PCB Prototyping Instrument on FR4 dielectric [130]. Figs. 5.14(a), 5.14(b) and 5.14(c) illustrate the three dimensional (3D) view of the proposed structure, top view of the standard patch with a 50Ω SMA connector and the AMC surface, respectively. The Keysight FieldFox Vector Network Analyzer (VNA) N9951A [154] has been used to measure the antenna performances in the anechoic chamber, as shown in Fig. 5.15(a). The broadband horn antenna [155] is employed as the receiving antenna, while the proposed prototype is used as the transmitting one, as illustrated in Figs. 5.15(b) and 5.15(c), respectively.

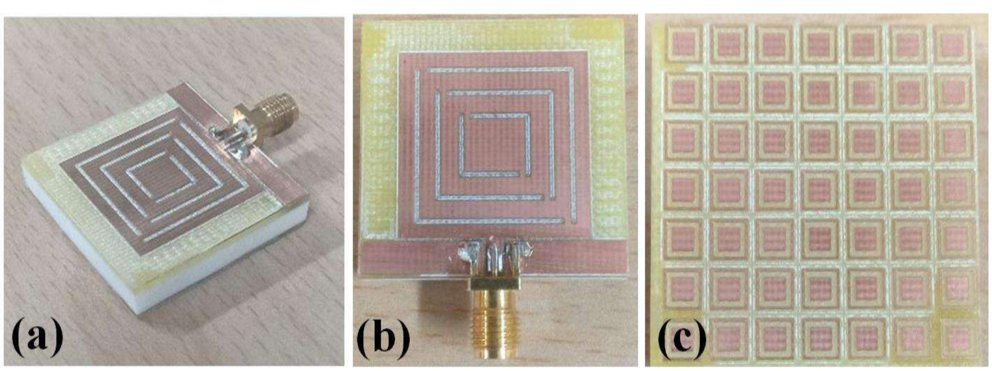

Fig. 5.14. Fabricated structure of the proposed antenna with (a) three-dimensional (3D) view (b) top and (c) MS surface.

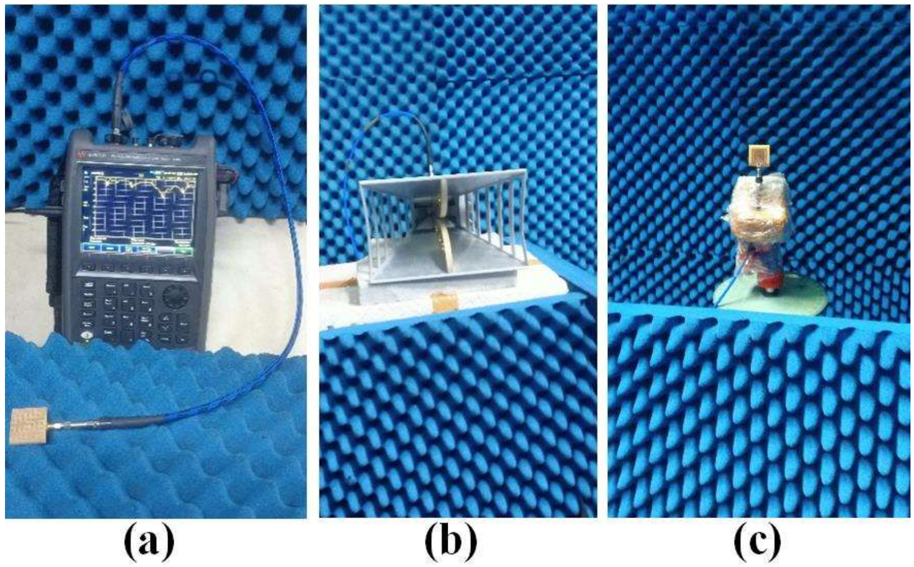

Fig. 5.15. Antenna measurement in an anechoic chamber (a) using VNA (b) broadband horn antenna and (c) the fabricated MSA under test.

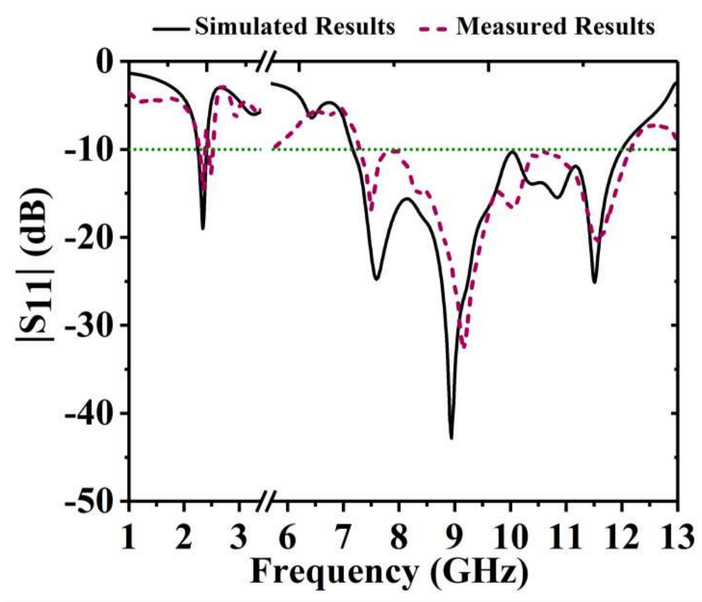

Fig. 5.16. The plot of the simulated and measured $|S_{11}|$ (dB) with respect to frequency.

The reflection coefficient characteristics have been measured for the developed prototype and consequently compared with the simulated result as shown in Fig. 5.16(a). It has been experimentally verified that an impedance bandwidth of -10 dB has been realized in the frequency ranges 2.27 GHz-2.41 GHz and 7.26 GHz-12.04 GHz while a maximum return loss of 33 dB has been observed at 9.1 GHz; thereby mimicking the simulated response. The analysis of the surface current distributions of the CPW-fed patch and the AMC surface have been carried out at 2.34 GHz, 11.52 GHz and 11.98 GHz as illustrated in Fig. 5.17(a) and Fig. 5.17(b) respectively. The area between the patch surface contact and the CPW feed has a higher density of surface currents. Nevertheless, the field distribution is highest in the vicinity of slots, as well as the patch and unit cell surface interfaces of the MS. As illustrated in Fig. 5.17(b), the directions of surface currents at the unit cell interface are parallel to each other, establishing a magnetic coupling between the adjacent unit cells.

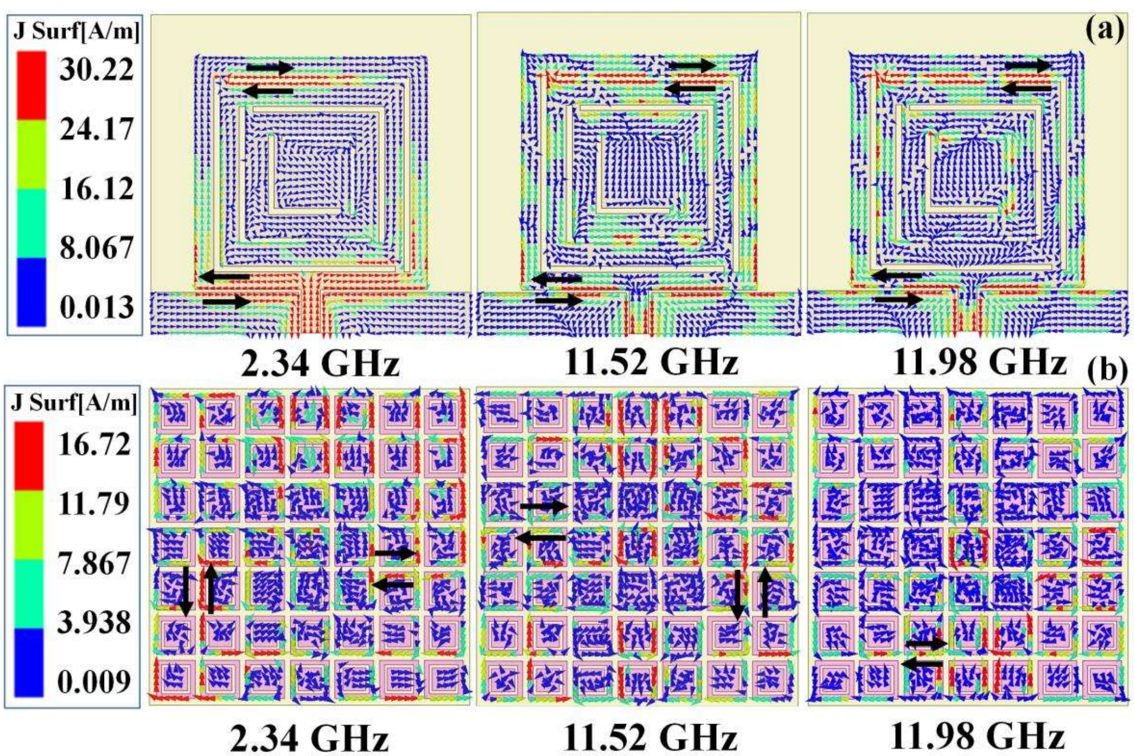

Fig. 5.17. Surface current distributions at (a) radiating patch (b) 7×7 order MS at different operating frequencies.

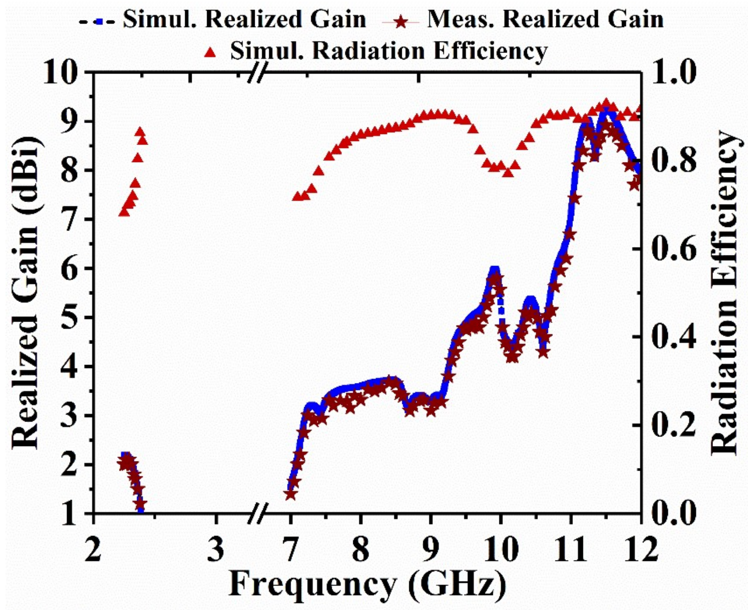

Fig. 5.18. Responses of realized gain (dBi) and radiation efficiency with respect to frequency.

The far-field gain characteristics of the antenna and radiation efficiencies are also shown in Fig. 5.18, where the measured parameters have been compared to the simulated ones and found to be in close agreement. The maximum simulated realized gain is 9.2 dBi, while the experimentally measured realized gain has been achieved as 9.1 dBi at 11.98 GHz. The AMC surface provides a gain improvement of nearly 5 dB over the standard patch, which has a maximum realized gain of 4.3 dBi. Moreover, it can be seen from Fig. 5.18 that the designed antenna offers the maximum radiation efficiency of 91.2% at 11.98 GHz. Antenna losses like dielectric loss, conductor loss, and other losses are not included in this efficiency value, which rises to 91.2 % [74]. The actual radiation efficiency will be lower in practise. The radiation patterns are unstable over the operating bands may be due to leakage of out of phase fields from few slots at patch or the unit cells of the metasurface. The vector surface current distributions of the conventional patch and the proposed metasurface are shown in Fig. 5.17 at 2.34 GHz, 11.52 GHz, and 11.98 GHz, respectively. It can be observed that there is a strong coupling current both the radiating patch and the metasurface at 2.34 GHz while at 11.52 GHz and 11.98 GHz, the coupling currents are less in the slots of the patch and the unit cells of the metasurface. The presence of strong coupling currents in the device may be due to less interspacing of the unit cells. However, such distortion at high frequency is still acceptable for wireless hand held devices working at multipath environment as the proposed antenna's cross-polarized levels remain lower than the co-polarized ones in the boresight direction.

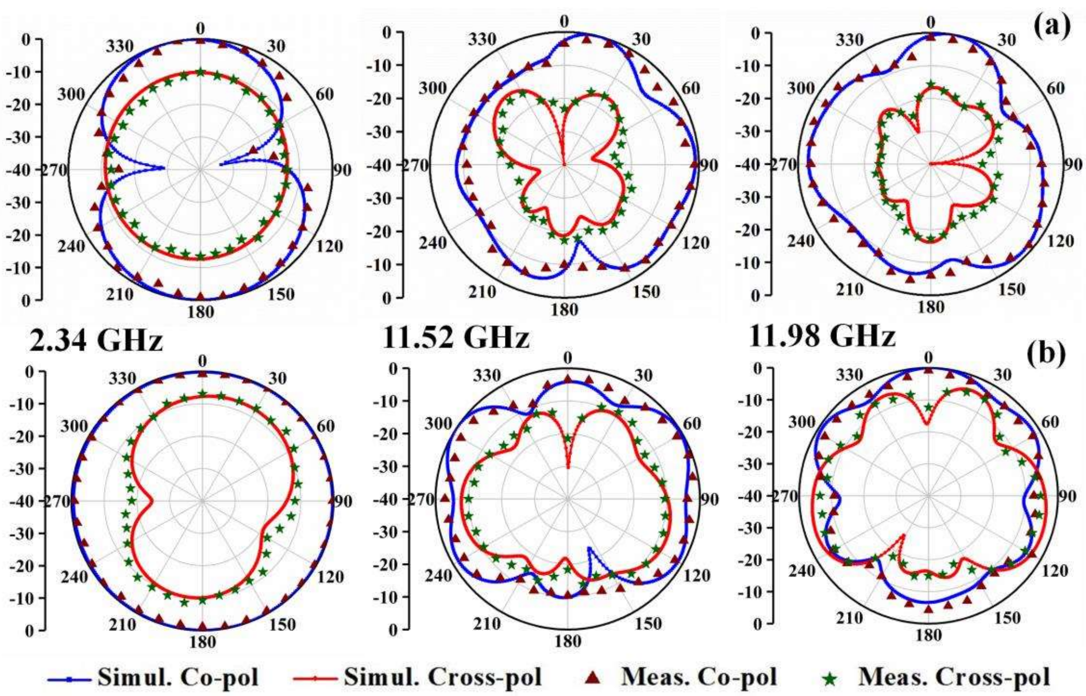

Fig. 5.19. Radiation patterns in the (a) E-plane and (b) H- plane at frequencies of 2.34 GHz, 11.52 GHz and 11.98 GHz.

Figs. 5.19(a) and 5.19(b) depict the simulated and experimental radiation patterns of the proposed antenna along with the E- and H-planes at 2.34 GHz, 11.52 GHz, and 11.98 GHz, respectively. This antenna has directional radiation characteristics that radiate along the boresight direction in both planes at all the operating frequencies as seen from Fig. 5.19.

Moreover, at all operational frequencies, the cross-polarized levels of the proposed antenna are at least 10 dB lower than the co-polarized ones. The simulated and experimental values differ slightly, which might be attributed to the manufacturing limitations such as FR4 dielectric copper loss during polishing, soldering between the copper layer and SMA connector, dielectric loss, adapter, and cable losses incurred during far-field testing.

TABLE 5.1. Comparison of the Proposed Work with Some Existing Antennas

Ref.	**Overall Dimensions**	**Frequencies (GHz)**	**Fractional BW (%)**	**Maximum Gain (dBi)**	**Maximum Efficiency (%)**	**Antenna Type**
[114]	$0.83\lambda_0\times0.83\lambda_0\times0.08\lambda_0$	2.4/5.2	15.6/ 9.3	7.3	65	AMC Reflector
[180]	$1.3\lambda_0\times0.9\lambda_0\times0.14\lambda_0$	2.6/3.5	7.7/5.7	8.6	88	Metasurface based two closely packed antenna
[181]	$0.9\lambda_0\times0.9\lambda_0\times0.29\lambda_0$	10.44	7.66	7.57	_	Superstrate type metasurface structure
[187]	$2.22\lambda_0\times0.75\lambda_0\times0.05\lambda_0$	3.5/4.9	8.5/4.08	12.43	_	Metasurface Antenna
[189]	$0.71\lambda_0\times0.71\lambda_0\times0.101\lambda_0$	5.25/6.6	43.9	8.4	92	AMC Type
[190]	$0.68\lambda_0\times0.68\lambda_0\times0.04\lambda_0$	1.57/2.45	7.6/ 5.5	1.99	83	AMC Backing
[193]	$0.93\lambda_0\times0.93\lambda_0\times0.13\lambda_0$	3.5/4.9	19.8/ 13.2	8.2	90	AMC Type
[194]	$0.75\lambda_0\times0.75\lambda_0\times0.027\lambda_0$	2.45/5.8	9.6/ 12.4	4.88	_	AMC Reflector
This Work	$0.25\lambda_0\times0.25\lambda_0\times0.06\lambda_0$	2.34/8.94	6.8/53.8	9.1	91.2	Slotted patch with AMC surface

The performance of the proposed MSA has also been compared to various other previously reported high-performance antennas as illustrated in Table 5.1. It can be seen that the proposed low-profile antenna has substantially enhanced gain, as well as improved bandwidth and compactness. Although the antenna described in [187] has a higher gain, it has a limited bandwidth and poor radiation efficiency. Furthermore, the improved realized gain of the proposed antenna to 9.1 dBi has led to the enhancement of the radiation efficiency of this prototype to 91.2% by maintaining compactness in the design.

5.4. Concluding Remarks

This work presents a unique, low-profile, efficient, and high-performance dual-band antenna with an AMC surface. The proposed approach incorporates a slotted patch and a 7×7 array of periodic unit cells placed in a superstrate arrangement. A teflon material has been used to separate the AMC surface from the radiating patch. Here, the radiating element is placed on top of the first dielectric, while the MS layer has been positioned on top of the second dielectric. The antenna operates at two frequencies, 2.34 GHz and 8.94 GHz, with fractional bandwidths of 6.8% and 53.8%, respectively. At the operational frequencies, this antenna has an endfire pattern that radiates in both E- and H-planes simultaneously. It radiates toward the boresight, with a maximum realized gain of 9.1 dBi and a radiation efficiency of 91.2% at 11.98 GHz. The proposed prototype has been fabricated, and the experimentally measured parameters are in good resemblance with the simulated values. This antenna can be used in a variety of IoT applications, including WMAX/WLAN, civil and military surveillance, and more.